ATMOSPHERIC SCIENCE

Large contribution to secondary organic aerosol from isoprene cloud chemistry

Houssni Lamkaddam[1]*, Josef Dommen[1], Ananth Ranjithkumar[2], Hamish Gordon[3], Günther Wehrle[1], Jordan Krechmer[4], Francesca Majluf[4], Daniil Salionov[5], Julia Schmale[1,6], Saša Bjelić[5], Kenneth S. Carslaw[2], Imad El Haddad[1]*, Urs Baltensperger[1]*

Aerosols still present the largest uncertainty in estimating anthropogenic radiative forcing. Cloud processing is potentially important for secondary organic aerosol (SOA) formation, a major aerosol component: however, laboratory experiments fail to mimic this process under atmospherically relevant conditions. We developed a wetted-wall flow reactor to simulate aqueous-phase processing of isoprene oxidation products (iOP) in cloud droplets. We find that 50 to 70% (in moles) of iOP partition into the aqueous cloud phase, where they rapidly react with OH radicals, producing SOA with a molar yield of 0.45 after cloud droplet evaporation. Integrating our experimental results into a global model, we show that clouds effectively boost the amount of SOA. We conclude that, on a global scale, cloud processing of iOP produces 6.9 Tg of SOA per year or approximately 20% of the total biogenic SOA burden and is the main source of SOA in the mid-troposphere (4 to 6 km).

INTRODUCTION

Aerosols and clouds play a vital role in Earth's energy budget (*1*). Organic aerosol (OA), a major fraction of the total submicrometer aerosol mass (20 to 50%), is overwhelmingly secondary (SOA; up to 90%), formed through gas-to-particle conversion of condensable oxidation products from gaseous precursors (*2*). While our knowledge of SOA production via gas-phase chemistry has substantially improved over the past decades, SOA production in clouds has received much less attention (*3*–*5*). Major SOA components, such as organic acids (*4*), shown to form in the aqueous phase during laboratory experiments (*3*, *6*), have been measured in the field at higher concentrations than expected from direct emissions or gas-phase oxidation (*7*–*9*). Current state-of-the-art models can reasonably predict OA measurements within the boundary layer close to emission sources but are subject to greater uncertainties with altitude, where most clouds exist (i.e., 1 to 6 km) (*10*). Despite the potential importance of cloud chemistry in modulating OA chemical composition and concentrations, the production of in-cloud aqueous SOA (aqSOA) remains virtually nonquantifiable because of major experimental limitations (e.g., simulation tool and mass spectrometer resolution and sensitivity) related to simulating aqueous chemistry at diluted conditions characteristic of atmospheric clouds.

Isoprene represents half of the flux of the biogenic volatile organic compounds emitted into the atmosphere (*11*). Although its SOA mass yield through gas-phase photooxidation is subject to vigorous debate, numerous publications (fig. S1) clearly show relatively low SOA mass yields (≤5% on average), with some outliers obtained under specific conditions (e.g., highly acidic seeds). Despite its low SOA yield, isoprene is presumed to be one of the largest SOA sources at the global scale because of its high emission rate (*12*, *13*). As its oxidation products are mainly water soluble (*14*), their chemical reactions in cloud water could constitute a substantial aqSOA source (*15*), and a neglected pathway that is competitive to SOA formation from the gas phase.

Here, we present the first experimental simulation of aqSOA formation from combined photochemistry and cloud chemistry from isoprene under atmospherically relevant conditions, using a newly developed wetted-wall flow reactor (WFR), which operates in continuous flow mode. The WFR was constructed in analogy to the "rotating wetted wall flow tube" from Hanson's group (*16*–*20*). Experiments were performed at 100% relative humidity (RH) and a temperature of 295 K; isoprene and its oxidation products were introduced into the WFR along with ozone, OH, and water vapor in the presence of light (case study A) and in the dark (case study B), where they were allowed to further react in the gas phase and in an aqueous microfilm (Materials and Methods and fig. S2). We used state-of-the-art mass spectrometers to fully characterize the properties of the formed organic molecules, such as yields, volatility, and solubility. Measurements were made online in the gas phase and offline in the liquid phase through subsequent nebulization of the aqueous solutions. AqSOA yields and production rates were determined, parameterized, and implemented into the atmosphere-only configuration of the U.K. Earth System Model (UKESM1). We used the U.K. Chemistry and Aerosol Model (*21*, *22*) of UKESM1 to assess the impact of isoprene chemistry in cloud water on the global SOA burden.

RESULTS AND DISCUSSION

Experimental findings

We measured isoprene and its gaseous oxidation products with a proton transfer reaction time-of-flight mass spectrometer (PTR-TOF-MS) and an acetate chemical ionization mass spectrometer (acetate-CIMS). Upon the rapid consumption of 8.4 parts per billion by volume (ppb_v) of isoprene by OH radicals, oxidized vapors are formed, accounting for 98 ± 14% (1σ) of the total reacted carbon (phase II of case study A; Fig. 1A). Note that as in the ambient environment,

[1]Laboratory of Atmospheric Chemistry, Paul Scherrer Institute, 5232 Villigen, Switzerland. [2]School of Earth and Environment, University of Leeds, Leeds LS2 9JT, UK. [3]Engineering Research Accelerator, Carnegie Mellon University, Pittsburgh 15213, USA. [4]Aerodyne Research Inc., Billerica, MA 01821, USA. [5]Bioenergy and Catalysis Laboratory, Paul Scherrer Institute, 5232 Villigen, Switzerland. [6]School of Architecture, Civil and Environmental Engineering, École Polytechnique Fédérale de Lausanne, Lausanne, Switzerland.
*Corresponding author. Email: houssni.lamkaddam@psi.ch (H.L.); imad.el-haddad@psi.ch (I.E.H.); urs.baltensperger@psi.ch (U.B.)

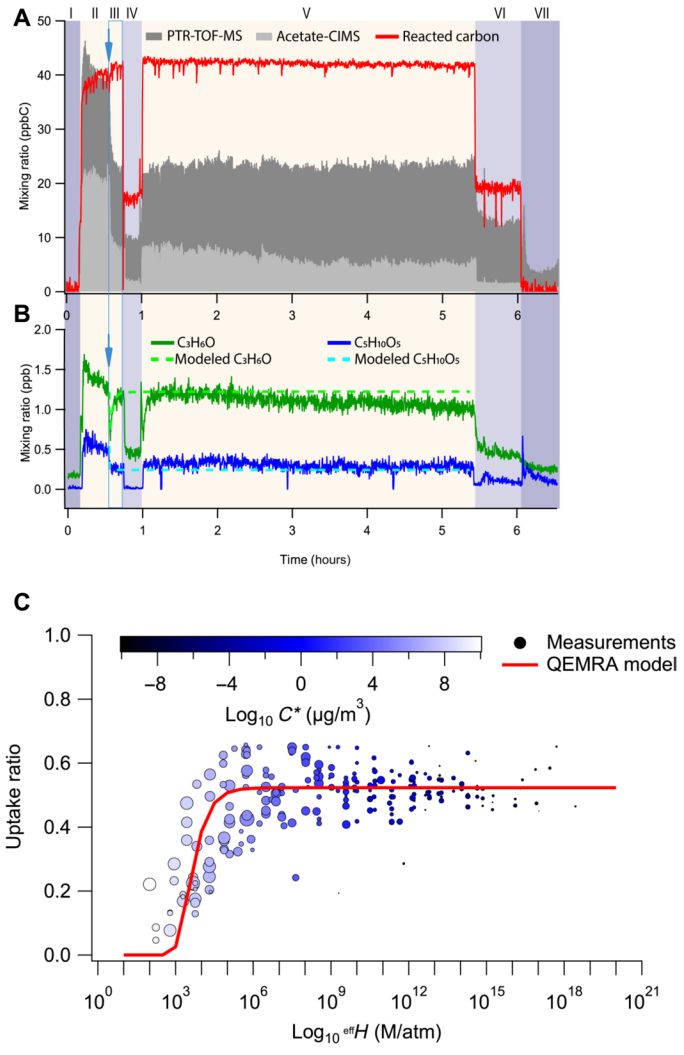

Fig. 1. Time series of isoprene oxidation products measured by mass spectrometry for a case study of type A and solubility-dependent uptake ratio. The experiment consists of six phases (all at 100% RH and 295 K). Phase I: Conditioning of the WFR flow tube in the dark to reach a steady state mixing ratio of 10 ppb_v isoprene. Phase II: Initiation of the photooxidation by switching on the Xe-excimer lamps (in front of the WFR) and the ultraviolet B (UVB) lamps (around the WFR). Phase III: Injection of the water microfilm, denoted by the blue arrow. Phase IV: OH oxidation of isoprene only with the Xe-excimer lamps, bypassing the WFR. Phase V (same as phase III): Reaction mixture through WFR with both the Xe-excimer and UVB lamps on and the water microfilm present. Phase VI: UVB lights off. Phase VII: Both Xe-excimer and UVB lamps off. (**A**) Carbon mass balance of the gas phase derived from PTR-TOF-MS and acetate-CIMS. The red line presents the isoprene decay measured by the PTR-TOF-MS, indicating 42-ppb_vC reacted isoprene carbon (corresponding to 8.4 ppb_v of consumed isoprene). Gray stacked areas denote the increase of unique oxidation products measured by both the PTR-TOF-MS (dark gray) and the acetate-CIMS (light gray), with molecules encountered in both instruments only being counted via the PTR-TOF-MS. Ions with the same molecular formula from both instruments comprised 2.8 ± 0.7 ppb_vC, indicating only 7 ± 2% of carbon overlap. (**B**) Measured (solid lines) and modeled (dashed lines; using the QEMRA model and calculated ^{eff}H values) evolution of selected nonsoluble (C_3H_6O) and soluble ($C_5H_{10}O_5$) oxidation products. (**C**) Representative uptake ratio after 5 hours of cloud processing as a function of the effective Henry's law constant (^{eff}H) color coded with the saturation vapor concentration (C^*).

WFR experiments simulate low NO_x conditions where HO_2-derived products such as isoprene epoxydiol (IEPOX) and hydroxy hydroperoxide (ISOPOOH) concentrations represent the atmospheric daytime conditions well (see the Supplementary Materials for detailed calculations) (*23*).

Once steady state was reached, we experimentally simulated the presence of cloud water by generating an aqueous microlayer on the WFR wall (Fig. 1A, phase III). A sudden decrease of the concentrations of the oxidation products was observed, demonstrating their uptake into the microfilm. Figure 1B shows the time dependence of representative species with different solubility. Less soluble compounds such as C_3H_6O quickly reach their aqueous saturation concentration, and their mixing ratios in the gas phase increase back to their initial values. More soluble compounds such as $C_5H_{10}O_5$ experience a continuous and irreversible uptake. The uptake ratio ($[C_{ClearAir} - C_{Cloud}]/C_{ClearAir}$) was calculated for all detected gaseous species, after, e.g., 5 hours of cloud simulation, and is displayed in Fig. 1C against their effective Henry's law solubility constant (^{eff}H, in M atm^{-1}). ^{eff}H was estimated on the basis of the compounds' elemental composition using structure activity relationships [i.e., GROupcontribution Method for Henry's law Estimate (GROMHE) (*24*); see the Supplementary Materials]. We have developed the kinetic model QEMRA (aqueous-hydrometeor phase processing and mass transfer model; see the Supplementary Materials), which describes the partitioning of molecules of different solubility. The model captures the experimental data accurately, validating the estimated ^{eff}H. According to the model, 54% of the reaction mixture diffuses to the surface of the water microlayer, of which 91 ± 13% fully dissolve therein; the remaining fraction consisting of nonsoluble and nondiffused species escapes the WFR in the gas phase. Efficient uptake (≥95% of the maximum uptake) is observed for compounds with $^{eff}H > 10^5$ M atm^{-1}, close to atmospheric cloud conditions, where one finds notable partitioning for species with $^{eff}H \geq 10^7$ M atm^{-1} (fig. S3) (*25*). The aqueous OH radical concentrations and the median estimates (in cases A and B) of the total dissolved organic material reached after several hours of reaction are very similar to those found in atmospheric clouds (*6*), ranging between 1×10^{-11} and 6×10^{-13} M OH and between 122 and 40 μM organics, respectively. Previous aqSOA experiments, based on bulk solution, were conducted using highly concentrated mixtures (around millimolar), characteristic of wet aerosols rather than cloud water (around micromolar), and they were often restricted to the processing of single oxygenated molecules. Furthermore, they unrealistically favored molecules with only slight solubility [with ^{eff}H as low as 10^{-5} M atm^{-1} (*3*, *25*)], suggesting a poor representation of the chemical composition of the dissolved organic matter in cloud droplets and thus affecting the resulting chemistry (see fig. S3). In an attempt to study the aqueous processing under more realistic conditions, Brégonzio-Rozier *et al.* (*26*) used laboratory-generated cloud droplets, where the short lifetimes of these droplets (<10 min) and losses to the chamber walls prevented a quantitative assessment of aqSOA production yields. To the best of our knowledge, our experimental setup allows the first investigation of the partitioning of organic vapors at the air-water interface under near-ambient conditions. It provides a near-atmospheric simulation of the gas-phase radical chemistry at low NO_x conditions, the product distribution in the gas phase, the product/oxidant levels and distributions in clouds, the typical exposure times to clouds (~hours), and the full range of complexity found in oxidation mixtures.

After several hours of aqueous phase processing, the water mixture was collected, spiked with a solution of $(NH_4)_2SO_4$ (used as internal standard), nebulized, and dried, resulting in several micrograms per cubic meter of OA detected by an aerosol mass spectrometer (AMS). Nebulization of aqueous solutions produced during control runs following the same experimental procedure (see also the Supplementary Materials), but in the absence of isoprene, showed no detectable OA mass, demonstrating that the formed aqSOA is driven by isoprene oxidation and not affected by contamination in the reaction vessel. AqSOA bulk and detailed molecular composition were characterized by an AMS and an extractive electrospray ionization time-of-flight mass spectrometer (EESI-TOF-MS) (*27*), respectively, and used to identify the pathway by which the observed aqSOA was produced. Since the chemical composition for case studies of type A and B was found to be very similar (see fig. S4), the following discussion will only focus on case A.

The aqSOA AMS spectrum is characteristic of an aged OA with high contribution from oxygenated fragments, such as CO_2^+ and $C_2H_3O^+$ (Fig. 2A), and an atomic oxygen-to-carbon (O:C) ratio of

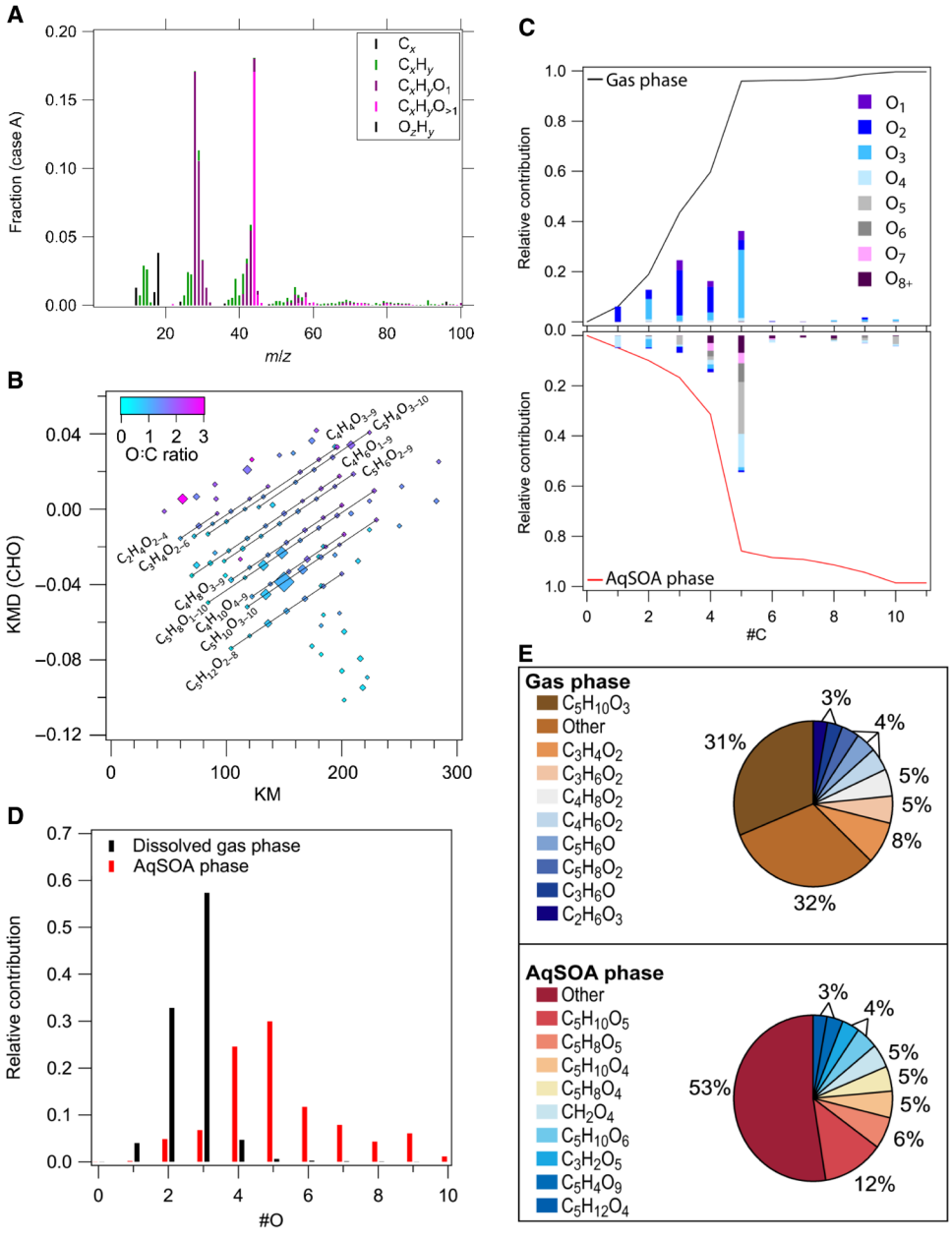

Fig. 2. Measured gaseous and aqSOA phase composition for a case study A. (**A**) Representative AMS spectrum and (**B**) Kendrick mass defect (KMD) plot (with CHO as unit base) of aqSOA determined from the EESI-TOF-MS. (**C**) Detailed chemical composition of the gas (top;, measured by the PTR-TOF-MS and the acetate-CIMS) and aqSOA (bottom; measured by the EESI-TOF-MS after nebulization) phase. Oxidation products are binned according to carbon number (*x* axis) and color coded by the oxygen number. (**D**) Relative contributions (in moles) of isoprene oxidation products in aqSOA and in the gas phase that dissolved into the WFR water microlayer, as a function of their oxygen number. (**E**) Relative contributions (in moles) of different compounds to the total gas (top) and aqSOA phase. The "other" group is composed of numerous compounds that each make up, at most, a few percent of the total.

1.1 ± 0.1, higher than typical values reported (~0.8) for laboratory-generated SOA from isoprene photooxidation in the gas phase (*28*). While acid-catalyzed reactions of IEPOX have been shown to be important for wet aerosols (*29*), the absence of an AMS signal at $C_5H_6O^+$ characteristic of IEPOX SOA (*30*) demonstrates that this is not the major aqSOA formation mechanism. These reactions require very low pH (<3) levels but are extremely slow at the pH range typical of cloud water and of our experiments (4 < pH < 7) (*15*). We estimate that the acid-catalyzed hydrolysis lifetime of IEPOX [$\tau_H = 1/(k_{H+}[H^+] + k_{nuc}[nuc][H^+])$], with the nucleophile concentration [nuc] ≡ [H_2O] = 55.55 M, $k_{H+} = 3.6 \times 10^{-2}$ M^{-1} s^{-1} (*31*), and $k_{nuc} = 2 \times 10^{-4}$ M^{-2} s^{-1} (*32*) would still be 59 hours, when considering the lowest pH (~4) reached under our conditions.

The aqSOA molecular composition determined by the EESI-TOF-MS is shown in Fig. 2B as a unit-CHO–based Kendrick mass defect plot and compared with the gas-phase reaction mixture in Fig. 2 (C to E). Homologous series of monomer (C ≤ 5) compounds constitute the major aqSOA fraction (84%), indicating that oligomerization plays a minor role in the formation of aqSOA, as expected from the diluted cloud conditions (*25*).

The aqSOA composition retrieved from the EESI-TOF is again highly oxygenated, with an average O:C ratio of 1.1, in excellent agreement with its bulk properties determined by the AMS. The top 10 molecules, accounting for 47% of the total aqSOA, are highly oxygenated monomers having four to six oxygen atoms, whereas the major gas-phase molecules contain only two to three oxygen atoms (average O:C ratio of 0.6) (Fig. 2, D and E). The oxygen number (#O) per molecule in aqSOA species is significantly higher than #O of species dissolved into the WFR water microlayer (determined as the difference in the gas-phase composition with and without the water microfilm). This shows that the dissolution of isoprene oxidized vapors cannot explain the aqSOA production and provides strong evidence that aqSOA results from OH reactions of the dissolved species in the aqueous phase. As an example, we estimate the lifetime

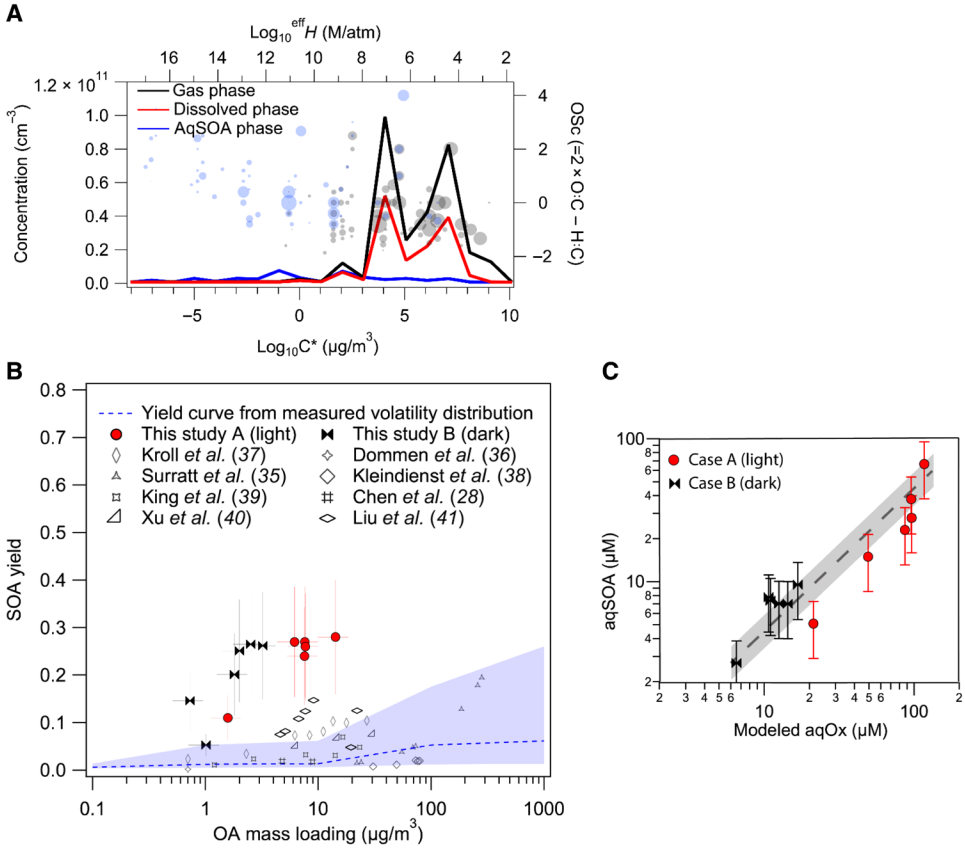

Fig. 3. Multiphase volatility distribution and SOA formation by in-cloud processing. (**A**) Volatility distribution of the oxidation products in the gas phase in the absence of the water microfilm (dark line; measured by the PTR-TOF-MS and the acetate-CIMS), of the aqSOA phase (blue line; measured by the EESI-TOF), and representative dissolved phase (red line; calculated from the QEMRA model after 10 hours of experiment). The oxidation state (OSc) is presented on the right axis. (**B**) SOA formation yield from cloud processing of isoprene oxidation products (filled markers), compared to our own SOA from gas phase oxidation (dashed line) and literature data from isoprene photooxidation laboratory experiments at low-NO_x conditions (open markers). The dashed line represents the yield determined from the measured volatility distribution in the gas phase [see (A)], where the shaded area indicates the response of the yield to a shift of the volatility bins by one order of magnitude. (**C**) Measured aqSOA molar concentration as a function of modeled aqueous oxidation products in the WFR microlayer. A linear fit parameterization ($y = 0.45 \times x$), using a least-square method, is represented by the dashed line. The error (2σ) of the fit is represented by the shaded area. The OH concentrations at steady-state conditions are as follows: case A (light), 2×10^9 molecules cm^{-3} in the gas phase and 4×10^{-13} to 3×10^{-11} M in the aqueous phase; case B (dark), 3×10^8 molecules cm^{-3} in the gas phase and 3×10^{-13} to 5×10^{-12} M in the aqueous phase. The aqueous OH concentration compares well to typical ambient conditions in cloud droplets [10^{-14} to 10^{-12} M (*6*)]. Note that the high OH dose in the gas phase is needed to initiate a sufficient concentration of oxidation products but does not result in atmospherically irrelevant conditions (see the Supplementary Materials for details).

of IEPOX toward aqueous OH reaction [$\tau_{aqOH} = 1/(k_{aqOH}[OH]$, with [OH] = 10^{-12} M and $k_{aqOH} = 1.4 \times 10^9$ M^{-1} s^{-1} (*33*)] to be only 12 min, substantially faster than its acid-catalyzed hydrolysis. Accordingly, 2-methylglyceric acid, recently identified as a reaction product of IEPOX with OH in the aqueous phase (*33*, *34*), was identified in our study (fig. S5) on the basis of tandem mass spectrometry analysis. Similar to IEPOX, dissolved isoprene oxidation products rapidly react with OH to yield products with much higher oxidation state, forming aqSOA.

The increase in the oxidation state of isoprene gas-phase oxidation products through further OH oxidation in the aqueous phase is expected to translate into a significant decrease in their volatility. Figure 3A presents the effective saturation vapor concentrations (C^*, in μg m^{-3}) and the oxidation states of the molecules in the aqSOA and those that dissolved from the gas phase into the aqueous microlayer. The majority of isoprene oxidation products in the gas phase (91.1 ± 10.3%) are highly volatile (C^* > 300 μg m^{-3}), and only a minor fraction (1.7 ± 0.4% of the total carbon budget) has sufficiently low volatility (C^* < 0.3 μg m^{-3}) to form SOA under atmospherically relevant conditions. Calculated SOA yields based on the volatility distribution of the isoprene oxidation products in the gas phase (Fig. 3B) are generally consistent with the low SOA yields reported in literature (*28*, *35*–*42*). For comparison, we estimate the

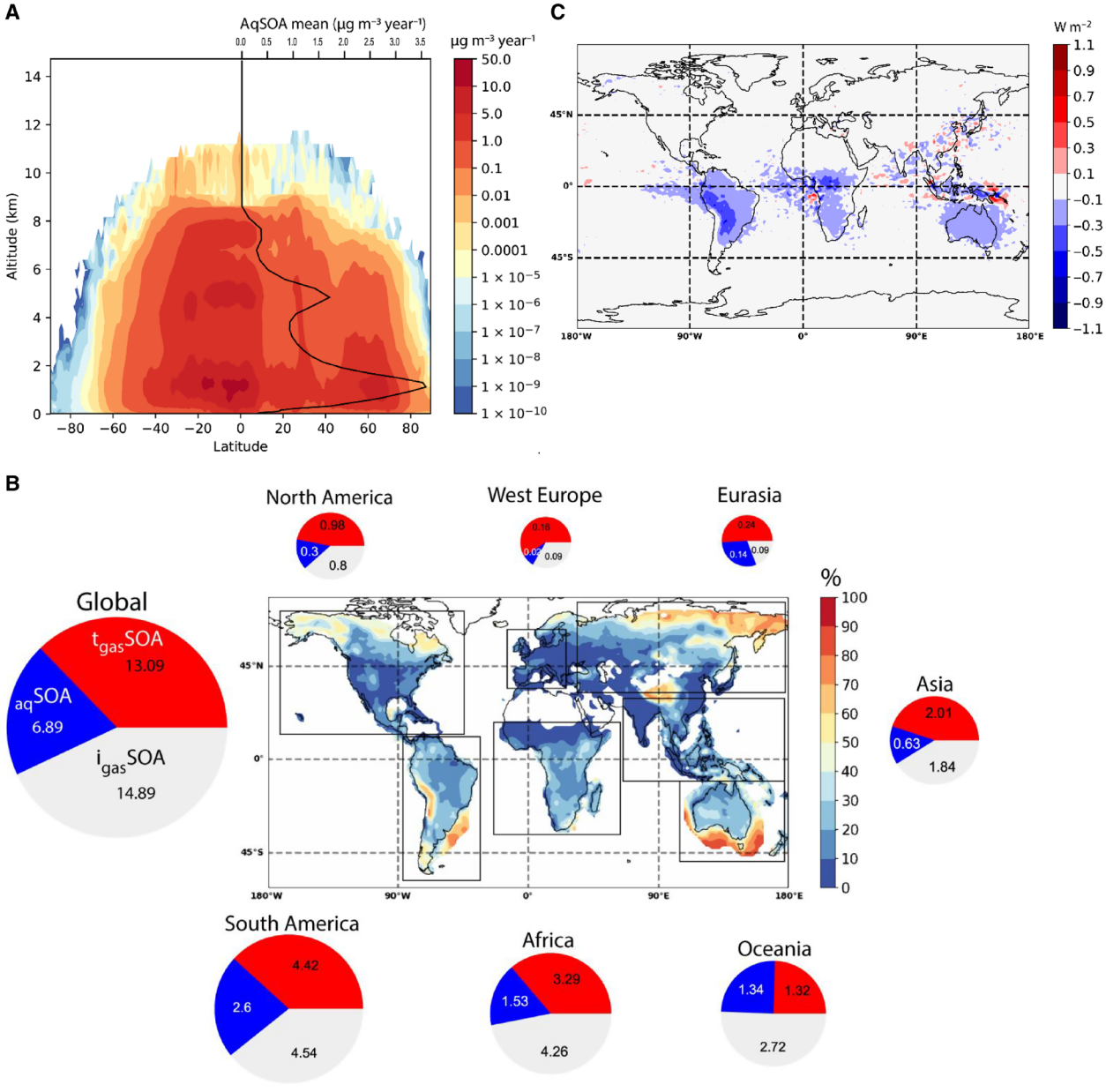

Fig. 4. aqSOA mass concentration due to isoprene cloud chemistry. (**A**) Simulated longitudinal mean vertical profile of the SOA formation rate from aqueous phase isoprene cloud chemistry. (**B**) Relative change in global SOA mass formation rate after implementing isoprene cloud chemistry, where the pie charts represent the total mass of SOA formed (in Tg $year^{-1}$) via three different pathways: terpene ($t_{gas}SOA$) or isoprene ($i_{gas}SOA$) gas-phase SOA formation and isoprene cloud processing (aqSOA) over the entire globe and over each continental area that is marked on the map with a box. Where the total SOA formation rate is below 1 Tg $year^{-1}$, the change is masked (white on the map). (**C**) Change in the direct radiative effect of aerosols at the top of the atmosphere when aqSOA is implemented in the model.

multiphasic SOA yield as the ratio between the aqSOA mass measured by the AMS and the integrated mass of the gaseous isoprene oxidation products that diffused to the WFR wetted wall. Multiphasic SOA yield values range from 0.05 to 0.28 at a load of 1 to 10 μg m^{-3}, at least twice as high compared to reported gas-phase SOA yields and yields calculated from the volatility distribution of isoprene oxidation products in the gas phase. To the best of our knowledge, this is the first experimental demonstration of enhanced SOA production through OH oxidation in simulated cloud droplets. Figure 3C shows the strong relationship between the measured aqSOA and the total reacted products in the liquid phase estimated using QEMRA, confirming that aqSOA derives from the reaction of isoprene products with OH radicals in the aqueous phase. The fraction of the isoprene oxidation products that dissolve into the aqueous microlayer amounts to ~50% of the total gas phase, under our conditions (shown as the red line in Fig. 3A). Once in the aqueous phase, these compounds rapidly react with OH, with lifetimes of minutes under atmospherically relevant conditions: ~5 min for case A and ~70 min for case B, assuming a well-constrained generic reaction rate constant toward OH of $k_{OH\text{-}aq}$ $(3.8 \pm 1.9) \times 10^8$ M^{-1} s^{-1} (*43*). On the basis of the linear fit of the data in Fig. 3C, we estimate that 45 ± 11% of the species that reacted in the aqueous phase form aqSOA upon evaporation of the nebulized aqueous droplets. As aqueous concentrations of OH radicals and total organic species in our conditions are typical of values reported for atmospheric clouds (*44*, *45*), the observed reactivity and aqSOA formation under our experimental conditions are expected to match typical conditions in clouds.

Global model simulation and atmospheric implications

To assess the atmospheric implication of aqSOA formation from isoprene on a global scale, we implement the parameterizations of experimental data in the global climate model UKESM1. The uptake fraction of isoprene oxidation products in cloud droplets was parameterized as a function of liquid water content using our measured solubility distribution; it ranges between 50 and 70% under typical atmospheric conditions (see the Supplementary Materials and fig. S6). We also used a $k_{OH\text{-}aq}$ of 3.8×10^8 M^{-1} s^{-1} and the experimentally derived yield of 0.45 in the model. Figure 4 shows the spatial variation of aqSOA and its contribution to the total SOA budget at the global and continental level. AqSOA exerts a substantial impact on the vertical aerosol distribution (Fig. 4A). The most important SOA precursors in our model, monoterpenes, are relatively short-lived, so they produce SOA close to the ground, while the contribution of aqSOA is more important at higher altitudes where clouds are ubiquitous (4 to 6 km). The aqueous chemistry process accounts for 6.9 Tg of SOA annually or ~20% of the total biogenic SOA budget (Fig. 4B). Including aqSOA in the model changes the direct radiative effect of aerosols at the top of the atmosphere by up to around −0.5 W m^{-2} (Fig. 4C) in Central Africa and the Amazon over a 1-year simulation. In our model, SOA is produced in the gas phase mainly close to sources (see the Supplementary Materials). Underestimating gas-phase production in remote regions and overestimating it near sources may affect the local radiative effects, and our calculations should be refined in the future using a model with a more sophisticated SOA production mechanism. However, it is unlikely that these effects significantly influence global averages. Hence, the substantial effects that we simulate demonstrate the importance of representing isoprene cloud chemistry to help improve the ability of models to capture the magnitude and variability of aerosol in the free troposphere to quantify aerosol climate effects. The large source of aerosol mass from aqSOA is located mostly in the Southern Hemisphere (80% of total aqSOA), whereas most previous observations of SOA were made in North America, Asia, and Europe. Therefore, our study calls for more dedicated field measurements in the Southern Hemisphere to elucidate the role of aqSOA formation in past, present, and future climate systems.

Overall, our results represent the first step toward a better representation of in-cloud aqSOA formation under relevant conditions to be integrated in models. Obviously, further studies beyond the limited range of conditions presented here (e.g., room temperature and low NO_x regime) are needed. Hence, our novel method opens up new avenues of in-cloud chemistry investigation under various environmental conditions (e.g., high NO_x, low temperatures representative of tropospheric clouds, and low pH) and for other volatile organic compound precursors.

MATERIALS AND METHODS

Wetted-wall flow reactor

Aqueous phase processing experiments of isoprene OH-oxidation products were performed in a rotating WFR. Although similar devices have been described in the literature (*17*, *20*, *46*), only occasional studies on the uptake of individual compounds in a solution were performed, while, to our knowledge, such wetted-wall reactors were never used so far to investigate the uptake of a complex mixture of gas phase oxidation products including all reactants, presumably because of technological limitations. The WFR consists of a quartz glass cylinder (length, 125 cm; internal diameter, 6 cm) into which between 8 and 58 ml of water were injected and rotated (15 rotations/min) to maintain a 35- to 250-μm water microlayer on the wall. While a stirring bar (length, 123 cm; diameter, 3 mm) at the bottom of the cylinder helps mix the solution, it mainly facilitates the wetting of the wall and maintains the microfilm. Note that the inner surface was sandblasted to increase the wettability of the glass. Around the WFR, nine ultraviolet B (UVB) lamps (Philips lamp TL 40W/12 RS) were used in certain experiments to start the photochemistry. When all lamps were switched on, the NO_2 and O_3 photolysis rates were $J_{NO2} = 3.64 \times 10^{-3}$ s^{-1} and $J_{O1D} = 5.30 \times 10^{-3}$ s^{-1}. A ventilation-cooling device on top of the UVB lamps' frame allowed us to control the temperature at ±1.5°C during the experiments. In addition, the laboratory room temperature was regulated to 22 ± 2°C with an air conditioner.

WFR conditioning and experimental protocol

Between each experiment, the WFR was cleaned three times with ultrapure water (18.2 megohm·cm; Millipore) by rotating it with 500 ml of water for 30 min. The WFR walls were then heated with a heat gun to 200°C, while a pure dry air stream of 20 liter min^{-1} was maintained for 1 hour.

All experiments were performed with a stream of synthetic clean air (10 liter min^{-1}) by mixing nitrogen (8 liter min^{-1}) produced from the evaporation of pressurized liquid nitrogen (purity, >99.999%; Messer) and oxygen (2 liter min^{-1}; purity, >99.995%; Messer) from gas cylinders. This dry air stream was passed through a porous PTFE (polytetrafluoroethylene) GORE-TEX tube (Gore) immersed in ultrapure water to keep a constant RH of 100%.

OH radicals were produced by irradiating the humidified air stream with a Xe-excimer laser (7.2 eV, 172 nm), where photolysis

of H_2O and O_2 leads to the formation of not only OH radicals but also O_3 and HO_2 molecules (*47*). Isoprene was then injected from a gas cylinder [100 part per million by volume (ppm_v) in N_2; purity, >99%; Carbagas AG] and combined with the humidified air stream containing the OH radicals. In this way, OH oxidation was initiated 34 ms before entering the WFR. In certain experiments, UVB lights were also used as a source of additional OH radicals within the flow tube. The residence time in the WFR was 21 s. A description of the experimental setup is shown in fig. S2 (in the Supplementary Materials) for different case studies and is explained in the following. A summary of the experimental conditions is provided in table S1.

Case study A: Aqueous phase processing of water-soluble organic compounds in the presence of light

Aqueous phase uptake and photochemical processing was performed simultaneously, as shown in fig. S2A (in the Supplementary Materials). A flow of 10 ppb_v isoprene was reacted with OH radicals generated with the Xe-excimer laser, followed by reactive uptake in the water microfilm in the presence of UVB light. Here, aqueous phase uptake and photochemical processing occurred simultaneously, i.e., in the presence of UVB light.

Case study B: Aqueous phase uptake of water-soluble organic compounds in the absence of light

Isoprene was reacted in the dark with OH radicals generated with the Xe-excimer laser, as shown in fig. S2B (in the Supplementary Materials). This step allowed water-soluble compounds to be taken up by the water microfilm but with a reduced photochemical processing compared to case A.

Measurements

Temperature was measured with two thermocouples of type K, one positioned at the inlet and the second one at the outlet. RH was monitored with a hydroclip (Rotronic HygroClip) and a dew point mirror (EdgeTech DewPrime II). Mixing ratios of the parent hydrocarbon and its oxidation products were monitored at the exit of the WFR with a PTR-TOF-MS (Ionicon, Series 8000) and an acetate chemical ionization atmospheric pressure interface time-of-flight mass spectrometer (acetate-CIMS; Airmodus/Aerodyne, Tofwerk). In certain experiments, a Vocus PTR-TOF-MS (Tofwerk/Aerodyne) was also used to determine the mixing ratios of gaseous products. Ozone was measured with a commercial monitor (Monitor Labs Inc., 8810).

At the end of the experiment, water samples were collected and stored at 4°C until chemical analysis, which was performed within 24 hours. Offline aqueous-phase chemical composition analysis was explored with three different instruments. Liquid samples were atomized in N_2 using an Apex Q nebulizer (Elemental Scientific Inc., Omaha, NE 68131, USA) operating at 60°C. The resulting aerosol was dried by passing it through a Nafion drier (resulting in an RH of <30%; Perma Pure, Toms River, NJ 08755, USA) and subsequently analyzed by a high-resolution time-of-flight AMS (Aerodyne) and an EESI-TOF-MS (*27*). In addition, collected samples were analyzed with liquid chromatography with a column (150 mm by 2.1 mm; particle size, 2.6 μm; Accucore RP-MS; Thermo Fisher Scientific) and a precolumn (Accucore RP-MS Defender Guards included; 10 mm by 2.1 mm; particle size, 2.6 μm), coupled with an LTQ Orbitrap Velos mass spectrometer (Thermo Fisher Scientific). Analyses were performed at isocratic conditions, with two different mobile phases consisting of the following: (i) 0.05% ethylenediamine (v/v), 39.98% water (v/v), and 59.97% methanol (v/v) and (ii) 0.05% formic acid (v/v), 19.99% water (v/v), and 79.96% methanol (v/v). Spectra were detected in positive and negative mode. Collision-induced dissociation multistage mass spectrometry (MS^n; $n = 2$) was performed on the most intense precursor ions. Details on operation and calibration can be found in the Supplementary Materials.

SUPPLEMENTARY MATERIALS

Supplementary material for this article is available at http://advances.sciencemag.org/cgi/content/full/7/13/eabe2952/DC1

REFERENCES AND NOTES

1. IPCC, *Climate Change 2013: The Physical Science Basis* (2013).
2. J. L. Jimenez, M. R. Canagaratna, N. M. Donahue, A. S. H. Prevot, Q. Zhang, J. H. Kroll, P. F. De Carlo, J. D. Allan, H. Coe, N. L. Ng, A. C. Aiken, K. S. Docherty, I. M. Ulbrich, A. P. Grieshop, A. L. Robinson, J. Duplissy, J. D. Smith, K. R. Wilson, V. A. Lanz, C. Hueglin, Y. L. Sun, J. Tian, A. Laaksonen, T. Raatikainen, J. Rautiainen, P. Vaattovaara, M. Ehn, M. Kulmala, J. M. Tomlinson, D. R. Collins, M. J. Cubison, E. J. Dunlea, J. A. Huffman, T. B. Onasch, M. R. Alfarra, P. I. Williams, K. Bower, Y. Kondo, J. Schneider, F. Drewnick, S. Borrmann, S. Weimer, K. Demerjian, D. Salcedo, L. Cottrell, R. Griffin, A. Takami, T. Miyoshi, S. Hatakeyama, A. Shimono, J. Y. Sun, Y. M. Zhang, K. zepina, J. R. Kimmel, D. Sueper, J. T. Jayne, S. C. Herndon, A. M. Trimborn, L. R. Williams, E. C. Wood, A. M. Middlebrook, C. E. Kolb, U. Baltensperger, D. R. Worsnop, Evolution of organic aerosols in the atmosphere. *Science* **326**, 1525–1529 (2009).
3. B. Ervens, Modeling the processing of aerosol and trace gases in clouds and fogs. *Chem. Rev.* **115**, 4157–4198 (2015).
4. M. Hallquist, J. C. Wenger, U. Baltensperger, Y. Rudich, D. Simpson, M. Claeys, J. Dommen, N. M. Donahue, C. George, A. H. Goldstein, J. F. Hamilton, H. Herrmann, T. Hoffmann, Y. Iinuma, M. Jang, M. E. Jenkin, J. L. Jimenez, A. Kiendler-Scharr, W. Maenhaut, G. McFiggans, T. F. Mentel, A. Monod, A. S. H. Prévôt, J. H. Seinfeld, J. D. Surratt, R. Szmigielski, J. Wildt, The formation, properties and impact of secondary organic aerosol: Current and emerging issues. *Atmos. Chem. Phys.* **9**, 5155–5236 (2009).
5. B. Ervens, A. Sorooshian, A. M. Aldhaif, T. Shingler, E. Crosbie, L. Ziemba, P. Campuzano-Jost, J. L. Jimenez, A. Wisthaler, Is there an aerosol signature of chemical cloud processing? *Atmos. Chem. Phys.* **18**, 16099–16119 (2018).
6. H. Herrmann, T. Schaefer, A. Tilgner, S. A. Styler, C. Weller, M. Teich, T. Otto, Tropospheric aqueous-phase chemistry: Kinetics, mechanisms, and its coupling to a changing gas phase. *Chem. Rev.* **115**, 4259–4334 (2015).
7. G. E. Likens, E. S. Edgerton, J. N. Galloway, The composition and deposition of organic carbon in precipitation1. *Tellus B* **35**, 16–24 (1983).
8. L. R. Mazzoleni, B. M. Ehrmann, X. Shen, A. G. Marshall, J. L. Collett Jr., Water-soluble atmospheric organic matter in fog: Exact masses and chemical formula identification by ultrahigh-resolution fourier transform ion cyclotron resonance mass spectrometry. *Environ. Sci. Technol.* **44**, 3690–3697 (2010).
9. K. E. Altieri, B. J. Turpin, S. P. Seitzinger, Oligomers, organosulfates, and nitrooxy organosulfates in rainwater identified by ultra-high resolution electrospray ionization FT-ICR mass spectrometry. *Atmos. Chem. Phys.* **9**, 2533–2542 (2009).
10. A. Hodzic, P. Campuzano-Jost, H. Bian, M. Chin, P. R. Colarco, D. A. Day, K. D. Froyd, B. Heinold, D. S. Jo, J. M. Katich, J. K. Kodros, B. A. Nault, J. R. Pierce, E. Ray, J. Schacht, G. P. Schill, J. C. Schroder, J. P. Schwarz, D. T. Sueper, I. Tegen, S. Tilmes, K. Tsigaridis, P. Yu, J. L. Jimenez, Characterization of organic aerosol across the global remote troposphere: A comparison of ATom measurements and global chemistry models. *Atmos. Chem. Phys.* **20**, 4607–4635 (2020).
11. A. B. Guenther, X. Jiang, C. L. Heald, T. Sakulyanontvittaya, T. Duhl, L. K. Emmons, X. Wang, The model of emissions of gases and aerosols from nature version 2.1 (MEGAN2.1): An extended and updated framework for modeling biogenic emissions. *Geosci. Model Dev.* **5**, 1471–1492 (2012).
12. K. H. Bates, D. J. Jacob, A new model mechanism for atmospheric oxidation of isoprene: Global effects on oxidants, nitrogen oxides, organic products, and secondary organic aerosol. *Atmos. Chem. Phys.* **19**, 9613–9640 (2019).
13. S. Stadtler, T. Kühn, S. Schröder, D. Taraborrelli, M. G. Schultz, H. Kokkola, Isoprene-derived secondary organic aerosol in the global aerosol–chemistry–climate model ECHAM6.3.0–HAM2.3–MOZ1.0. *Geosci. Model Dev.* **11**, 3235–3260 (2018).
14. Y. Liu, A. Monod, T. Tritscher, A. P. Praplan, P. F. De Carlo, B. Temime-Roussel, E. Quivet, N. Marchand, J. Dommen, U. Baltensperger, Aqueous phase processing of secondary organic aerosol from isoprene photooxidation. *Atmos. Chem. Phys.* **12**, 5879–5895 (2012).
15. W. G. Tsui, J. L. Woo, V. F. McNeill, Impact of aerosol-cloud cycling on aqueous secondary organic aerosol formation. *Atmosphere* **10**, 666 (2019).

16. D. R. Hanson, E. R. Lovejoy, Heterogeneous reactions in liquid sulfuric acid: HOCl + HCl as a model system. *J. Phys. Chem.* **100**, 6397–6405 (1996).
17. E. R. Lovejoy, L. G. Huey, D. R. Hanson, Atmospheric fate of CF_3OH 2: Heterogeneous reaction. *J. Geophys. Res. Atmos.* **100**, 18775–18780 (1995).
18. D. J. Donaldson, A. R. Ravishankara, D. R. Hanson, Detailed study of HOCl + HCl → Cl_2 + H_2O in sulfuric acid. *J. Phys. Chem. A* **101**, 4717–4725 (1997).
19. B. Nozière, C. A. Longfellow, B. E. Henry, D. Voisin, D. R. Hanson, Uptake of nopinone by water: Comparison between aqueous-and gas-phase oxidation of organic compounds in the atmosphere. *Geophys. Res. Lett.* **28**, 1965–1968 (2001).
20. B. Nozière, D. Voisin, C. A. Longfellow, H. Friedli, B. E. Henry, D. R. Hanson, The uptake of methyl vinyl ketone, methacrolein, and 2-methyl-3-butene-2-ol onto sulfuric acid solutions. *J. Phys. Chem. A* **110**, 2387–2395 (2006).
21. O. Morgenstern, P. Braesicke, F. M. O'Connor, A. C. Bushell, C. E. Johnson, S. M. Osprey, J. A. Pyle, Evaluation of the new UKCA climate-composition model—Part 1: The stratosphere. *Geosci. Model Dev.* **2**, 43–57 (2009).
22. F. M. O'Connor, C. E. Johnson, O. Morgenstern, N. L. Abraham, P. Braesicke, M. Dalvi, G. A. Folberth, M. G. Sanderson, P. J. Telford, A. Voulgarakis, P. J. Young, G. Zeng, W. J. Collins, J. A. Pyle, Evaluation of the new UKCA climate-composition model—Part 2: The troposphere. *Geosci. Model Dev.* **7**, 41–91 (2014).
23. P. O. Wennberg, K. H. Bates, J. D. Crounse, L. G. Dodson, R. C. Mc Vay, L. A. Mertens, T. B. Nguyen, E. Praske, R. H. Schwantes, M. D. Smarte, J. M. St Clair, A. P. Teng, X. Zhang, J. H. Seinfeld, Gas-phase reactions of isoprene and its major oxidation products. *Chem. Rev.* **118**, 3337–3390 (2018).
24. T. Raventos-Duran, M. Camredon, R. Valorso, C. Mouchel-Vallon, B. Aumont, Structure-activity relationships to estimate the effective Henry's law constants of organics of atmospheric interest. *Atmos. Chem. Phys.* **10**, 7643–7654 (2010).
25. B. Ervens, B. J. Turpin, R. J. Weber, Secondary organic aerosol formation in cloud droplets and aqueous particles (aqSOA): A review of laboratory, field and model studies. *Atmos. Chem. Phys.* **11**, 22301–22383 (2011).
26. L. Brégonzio-Rozier, C. Giorio, F. Siekmann, E. Pangui, S. B. Morales, B. Temime-Roussel, A. Gratien, V. Michoud, M. Cazaunau, H. L. De Witt, A. Tapparo, A. Monod, J.-F. Doussin, Secondary organic aerosol formation from isoprene photooxidation during cloud condensation–evaporation cycles. *Atmos. Chem. Phys.* **16**, 1747–1760 (2016).
27. F. D. Lopez-Hilfiker, V. Pospisilova, W. Huang, M. Kalberer, C. Mohr, G. Stefenelli, J. A. Thornton, U. Baltensperger, A. S. H. Prevot, J. G. Slowik, An extractive electrospray ionization time-of-flight mass spectrometer (EESI-TOF) for online measurement of atmospheric aerosol particles. *Atmos. Meas. Tech.* **12**, 4867–4886 (2019).
28. Q. Chen, Y. Liu, N. M. Donahue, J. E. Shilling, S. T. Martin, Particle-phase chemistry of secondary organic material: Modeled compared to measured O:C and H:C elemental ratios provide constraints. *Environ. Sci. Technol.* **45**, 4763–4770 (2011).
29. J. D. Surratt, A. W. H. Chan, N. C. Eddingsaas, M. N. Chan, C. L. Loza, A. J. Kwan, S. P. Hersey, R. C. Flagan, P. O. Wennberg, J. H. Seinfeld, Reactive intermediates revealed in secondary organic aerosol formation from isoprene. *Proc. Natl. Acad. Sci. U.S.A.* **107**, 6640–6645 (2010).
30. W. W. Hu, P. Campuzano-Jost, B. B. Palm, D. A. Day, A. M. Ortega, P. L. Hayes, J. E. Krechmer, Q. Chen, M. Kuwata, Y. J. Liu, S. S. de Sá, K. McKinney, S. T. Martin, M. Hu, S. H. Budisulistiorini, M. Riva, J. D. Surratt, J. M. St. Clair, G. I.-V. Wertz, L. D. Yee, A. H. Goldstein, S. Carbone, J. Brito, P. Artaxo, J. A. de Gouw, A. Koss, A. Wisthaler, T. Mikoviny, T. Karl, L. Kaser, W. Jud, A. Hansel, K. S. Docherty, M. L. Alexander, N. H. Robinson, H. Coe, J. D. Allan, M. R. Canagaratna, F. Paulot, J. L. Jimenez, Characterization of a real-time tracer for isoprene epoxydiols-derived secondary organic aerosol (IEPOX-SOA) from aerosol mass spectrometer measurements. *Atmos. Chem. Phys.* **15**, 11807–11833 (2015).
31. N. C. Cole-Filipiak, A. E. O'Connor, M. J. Elrod, Kinetics of the hydrolysis of atmospherically relevant isoprene-derived hydroxy epoxides. *Environ. Sci. Technol.* **44**, 6718–6723 (2010).
32. N. C. Eddingsaas, D. G. VanderVelde, P. O. Wennberg, Kinetics and products of the acid-catalyzed ring-opening of atmospherically relevant butyl epoxy alcohols. *J. Phys. Chem. A* **114**, 8106–8113 (2010).
33. T. Otto, T. Schaefer, H. Herrmann, Aqueous-phase oxidation of *cis*-β-isoprene epoxydiol by hydroxyl radicals and its impact on atmospheric isoprene processing. *J. Phys. Chem. A* **123**, 10599–10608 (2019).
34. T. Otto, B. Stieger, P. Mettke, H. Herrmann, Tropospheric aqueous-phase oxidation of isoprene-derived dihydroxycarbonyl compounds. *J. Phys. Chem. A* **121**, 6460–6470 (2017).
35. J. D. Surratt, S. M. Murphy, J. H. Kroll, N. L. Ng, L. Hildebrandt, A. Sorooshian, R. Szmigielski, R. Vermeylen, W. Maenhaut, M. Claeys, R. C. Flagan, J. H. Seinfeld, Chemical composition of secondary organic aerosol formed from the photooxidation of isoprene. *J. Phys. Chem. A* **110**, 9665–9690 (2006).
36. J. Dommen, A. Metzger, J. Duplissy, M. Kalberer, M. R. Alfarra, A. Gascho, E. Weingartner, A. S. H. Prevot, B. Verheggen, U. Baltensperger, Laboratory observation of oligomers in the aerosol from isoprene/NO_x photooxidation. *Geophys. Res. Lett.* **33**, L13805 (2006).
37. J. H. Kroll, N. L. Ng, S. M. Murphy, R. C. Flagan, J. H. Seinfeld, Secondary organic aerosol formation from isoprene photooxidation. *Environ. Sci. Technol.* **40**, 1869–1877 (2006).
38. T. E. Kleindienst, M. Lewandowski, J. H. Offenberg, M. Jaoui, E. O. Edney, The formation of secondary organic aerosol from the isoprene + OH reaction in the absence of NO_x. *Atmos. Chem. Phys.* **9**, 6541–6558 (2009).
39. S. M. King, T. Rosenoern, J. E. Shilling, Q. Chen, Z. Wang, G. Biskos, K. A. McKinney, U. Pöschl, S. T. Martin, Cloud droplet activation of mixed organic-sulfate particles produced by the photooxidation of isoprene. *Atmos. Chem. Phys.* **10**, 3953–3964 (2010).
40. L. Xu, M. S. Kollman, C. Song, J. E. Shilling, N. L. Ng, Effects of NO_x on the volatility of secondary organic aerosol from isoprene photooxidation. *Environ. Sci. Technol.* **48**, 2253–2262 (2014).
41. J. Liu, E. L. D'Ambro, B. H. Lee, F. D. Lopez-Hilfiker, R. A. Zaveri, J. C. Rivera-Rios, F. N. Keutsch, S. Iyer, T. Kurten, Z. Zhang, A. Gold, J. D. Surratt, J. E. Shilling, J. A. Thornton, Efficient isoprene secondary organic aerosol formation from a non-IEPOX pathway. *Environ. Sci. Technol.* **50**, 9872–9880 (2016).
42. A. G. Carlton, C. Wiedinmyer, J. H. Kroll, A review of secondary organic aerosol (SOA) formation from isoprene. *Atmos. Chem. Phys.* **9**, 4987–5005 (2009).
43. B. Ervens, Progress and problems in modeling chemical processing in cloud droplets and wet aerosol particles, in *Multiphase Environmental Chemistry in the Atmosphere* (American Chemical Society, 2018), vol. 1299, chap. 16, pp. 327–345.
44. S. E. Paulson, P. J. Gallimore, X. M. Kuang, J. R. Chen, M. Kalberer, D. H. Gonzalez, A light-driven burst of hydroxyl radicals dominates oxidation chemistry in newly activated cloud droplets. *Sci. Adv.* **5**, eaav7689 (2019).
45. L. Deguillaume, T. Charbouillot, M. Joly, M. Vaïtilingom, M. Parazols, A. Marinoni, P. Amato, A.-M. Delort, V. Vinatier, A. Flossmann, N. Chaumerliac, J. M. Pichon, S. Houdier, P. Laj, K. Sellegri, A. Colomb, M. Brigante, G. Mailhot, Classification of clouds sampled at the puy de Dôme (France) based on 10 yr of monitoring of their physicochemical properties. *Atmos. Chem. Phys.* **14**, 1485–1506 (2014).
46. T. Wang, Z. Liu, W. Wang, M. Ge, Uptake kinetics of three epoxides into sulfuric acid solution. *Atmos. Environ.* **56**, 58–64 (2012).
47. U. Molteni, F. Bianchi, F. Klein, I. E. Haddad, C. Frege, M. J. Rossi, J. Dommen, U. Baltensperger, Formation of highly oxygenated organic molecules from aromatic compounds. *Atmos. Chem. Phys.* **18**, 1909–1921 (2018).
48. M. Graus, M. Müller, A. Hansel, High resolution PTR-TOF: Quantification and formula confirmation of VOC in real time. *J. Am. Soc. Mass Spectrom.* **21**, 1037–1044 (2010).
49. J. de Gouw, C. Warneke, Measurements of volatile organic compounds in the earth's atmosphere using proton-transfer-reaction mass spectrometry. *Mass Spectrom. Rev.* **26**, 223–257 (2007).
50. L. Cappellin, M. Probst, J. Limtrakul, F. Biasioli, E. Schuhfried, C. Soukoulis, T. D. Märk, F. Gasperi, Proton transfer reaction rate coefficients between H_3O^+ and some sulphur compounds. *Int. J. Mass Spectrom.* **295**, 43–48 (2010).
51. T. Jokinen, M. Sipilä, H. Junninen, M. Ehn, G. Lönn, J. Hakala, T. Petäjä, R. L. Mauldin III, M. Kulmala, D. R. Worsnop, Atmospheric sulphuric acid and neutral cluster measurements using CI-APi-TOF. *Atmos. Chem. Phys.* **12**, 4117–4125 (2012).
52. H. Junninen, M. Ehn, T. Petäjä, L. Luosujärvi, T. Kotiaho, R. Kostiainen, U. Rohner, M. Gonin, K. Fuhrer, M. Kulmala, D. R. Worsnop, A high-resolution mass spectrometer to measure atmospheric ion composition. *Atmos. Meas. Tech.* **3**, 1039–1053 (2010).
53. T. H. Bertram, J. R. Kimmel, T. A. Crisp, O. S. Ryder, R. L. N. Yatavelli, J. A. Thornton, M. J. Cubison, M. Gonin, D. R. Worsnop, A field-deployable, chemical ionization time-of-flight mass spectrometer. *Atmos. Meas. Tech.* **4**, 1471–1479 (2011).
54. F. L. Eisele, D. J. Tanner, Measurement of the gas phase concentration of H_2SO_4 and methane sulfonic acid and estimates of H_2SO_4 production and loss in the atmosphere. *J. Geophys. Res. Atmos.* **98**, 9001–9010 (1993).
55. J. Krechmer, F. Lopez-Hilfiker, A. Koss, M. Hutterli, C. Stoermer, B. Deming, J. Kimmel, C. Warneke, R. Holzinger, J. Jayne, D. Worsnop, K. Fuhrer, M. Gonin, J. de Gouw, Evaluation of a new reagent-ion source and focusing ion–molecule reactor for use in proton-transfer-reaction mass spectrometry. *Anal. Chem.* **90**, 12011–12018 (2018).
56. K. Sekimoto, S.-M. Li, B. Yuan, A. Koss, M. Coggon, C. Warneke, J. Gouw, Calculation of the sensitivity of proton-transfer-reaction mass spectrometry (PTR-MS) for organic trace gases using molecular properties. *Int. J. Mass Spectrom.* **421**, 71–94 (2017).
57. P. F. DeCarlo, J. R. Kimmel, A. Trimborn, M. J. Northway, J. T. Jayne, A. C. Aiken, M. Gonin, K. Fuhrer, T. Horvath, K. S. Docherty, D. R. Worsnop, J. L. Jimenez, Field-deployable, high-resolution, time-of-flight aerosol mass spectrometer. *Anal. Chem.* **78**, 8281–8289 (2006).
58. A. Vlachou, A. Tobler, H. Lamkaddam, F. Canonaco, K. R. Daellenbach, J.-L. Jaffrezo, M. C. Minguillón, M. Maasikmets, E. Teinemaa, U. Baltensperger, I. E. Haddad, A. S. H. Prévôt, Development of a versatile source apportionment analysis based on positive matrix factorization: A case study of the seasonal variation of organic aerosol sources in Estonia. *Atmos. Chem. Phys.* **19**, 7279–7295 (2019).
59. R. Bahreini, B. Ervens, A. M. Middlebrook, C. Warneke, J. A. de Gouw, P. F. De Carlo, J. L. Jimenez, C. A. Brock, J. A. Neuman, T. B. Ryerson, H. Stark, E. Atlas, J. Brioude, A. Fried,

J. S. Holloway, J. Peischl, D. Richter, J. Walega, P. Weibring, A. G. Wollny, F. C. Fehsenfeld, Organic aerosol formation in urban and industrial plumes near Houston and Dallas, Texas. *J. Geophys. Res. Atmos.* **114**, D00F16 (2009).
60. N. M. Donahue, S. A. Epstein, S. N. Pandis, A. L. Robinson, A two-dimensional volatility basis set: 1. Organic-aerosol mixing thermodynamics. *Atmos. Chem. Phys.* **11**, 3303–3318 (2011).
61. A. Hodzic, B. Aumont, C. Knote, J. Lee-Taylor, S. Madronich, G. Tyndall, Volatility dependence of Henry's law constants of condensable organics: Application to estimate depositional loss of secondary organic aerosols. *Geophys. Res. Lett.* **41**, 4795–4804 (2014).
62. S. E. Schwartz, Mass-transport considerations pertinent to aqueous phase reactions of gases in liquid-water clouds, in *Chemistry of multiphase atmospheric systems* (Springer, 1986), pp. 415–471.
63. C. Bozzetti, K. R. Daellenbach, C. Hueglin, P. Fermo, J. Sciare, A. Kasper-Giebl, Y. Mazar, G. Abbaszade, M. E. Kazzi, R. Gonzalez, T. Shuster-Meiseles, M. Flasch, R. Wolf, A. Křepelová, F. Canonaco, J. Schnelle-Kreis, J. G. Slowik, R. Zimmermann, Y. Rudich, U. Baltensperger, I. E. Haddad, A. S. H. Prévôt, Size-resolved identification, characterization, and quantification of primary biological organic aerosol at a European Rural Site. *Environ. Sci. Technol.* **50**, 3425–3434 (2016).
64. T. Jokinen, T. Berndt, R. Makkonen, V.-M. Kerminen, H. Junninen, P. Paasonen, F. Stratmann, H. Herrmann, A. B. Guenther, D. R. Worsnop, M. Kulmala, M. Ehn, M. Sipilä, Production of extremely low volatile organic compounds from biogenic emissions: Measured yields and atmospheric implications. *Proc. Natl. Acad. Sci. U.S.A.* **112**, 7123–7128 (2015).
65. A. V. Ivanov, S. Trakhtenberg, A. K. Bertram, Y. M. Gershenzon, M. J. Molina, OH, HO_2, and ozone gaseous diffusion coefficients. *J. Phys. Chem. A* **111**, 1632–1637 (2007).
66. R. Atkinson, D. L. Baulch, R. A. Cox, J. N. Crowley, R. F. Hampson, R. G. Hynes, M. E. Jenkin, M. J. Rossi, J. Troe; IUPAC Subcommittee, Evaluated kinetic and photochemical data for atmospheric chemistry: Volume II—Gas phase reactions of organic species. *Atmos. Chem. Phys.* **6**, 3625–4055 (2006).
67. M. E. Jenkin, J. C. Young, A. R. Rickard, The MCM v3.3.1 degradation scheme for isoprene. *Atmos. Chem. Phys.* **15**, 11433–11459 (2015).
68. D. Taraborrelli, M. G. Lawrence, J. N. Crowley, T. J. Dillon, S. Gromov, C. B. M. Groß, L. Vereecken, J. Lelieveld, Hydroxyl radical buffered by isoprene oxidation over tropical forests. *Nat. Geosci.* **5**, 190–193 (2012).
69. R. Sommariva, S. Cox, C. Martin, K. Borońska, J. Young, P. K. Jimack, M. J. Pilling, V. N. Matthaios, B. S. Nelson, M. J. Newland, M. Panagi, W. J. Bloss, P. S. Monks, A. R. Rickard, AtChem (version 1), an open-source box model for the master chemical mechanism. *Geosci. Model Dev.* **13**, 169–183 (2020).
70. Z. Tan, H. Fuchs, K. Lu, A. Hofzumahaus, B. Bohn, S. Broch, H. Dong, S. Gomm, R. Häseler, L. He, F. Holland, X. Li, Y. Liu, S. Lu, F. Rohrer, M. Shao, B. Wang, M. Wang, Y. Wu, L. Zeng, Y. Zhang, A. Wahner, Y. Zhang, Radical chemistry at a rural site (Wangdu) in the North China Plain: Observation and model calculations of OH, HO_2 and RO_2 radicals. *Atmos. Chem. Phys.* **17**, 663–690 (2017).
71. D. Mihelcic, F. Holland, A. Hofzumahaus, L. Hoppe, S. Konrad, P. Müsgen, H.-W. Pätz, H.-J. Schäfer, T. Schmitz, A. Volz-Thomas, K. Bächmann, S. Schlomski, U. Platt, A. Geyer, B. Alicke, G. K. Moortgat, Peroxy radicals during BERLIOZ at Pabstthum: Measurements, radical budgets and ozone production. *J. Geophys. Res. Atmos.* **108**, 8254 (2003).
72. H. Fuchs, T. Brauers, R. Häseler, F. Holland, D. Mihelcic, P. Müsgen, F. Rohrer, R. Wegener, A. Hofzumahaus, Intercomparison of peroxy radical measurements obtained at atmospheric conditions by laser-induced fluorescence and electron spin resonance spectroscopy. *Atmos. Meas. Tech.* **2**, 55–64 (2009).
73. Z. Tan, K. Lu, A. Hofzumahaus, H. Fuchs, B. Bohn, F. Holland, Y. Liu, F. Rohrer, M. Shao, K. Sun, Y. Wu, L. Zeng, Y. Zhang, Q. Zou, A. Kiendler-Scharr, A. Wahner, Y. Zhang, Experimental budgets of OH, HO_2, and RO_2 radicals and implications for ozone formation in the Pearl River Delta in China 2014. *Atmos. Chem. Phys.* **19**, 7129–7150 (2019).
74. H. Fuchs, F. Holland, A. Hofzumahaus, Measurement of tropospheric RO_2 and HO_2 radicals by a laser-induced fluorescence instrument. *Rev. Sci. Instrum.* **79**, 084104 (2008).
75. M. Hanke, J. Uecker, T. Reiner, F. Arnold, Atmospheric peroxy radicals: ROXMAS, a new mass-spectrometric methodology for speciated measurements of HO_2 and $\cdot RO_2$ and first results. *Int. J. Mass Spectrom.* **213**, 91–99 (2002).
76. P. J. Ziemann, R. Atkinson, Kinetics, products, and mechanisms of secondary organic aerosol formation. *Chem. Soc. Rev.* **41**, 6582–6605 (2012).
77. S. Madronich, S. Flocke, The role of solar radiation in atmospheric chemistry, in *Environmental Photochemistry* (Springer, 1999), pp. 1–26.
78. E. O. Edney, T. E. Kleindienst, M. Jaoui, M. Lewandowski, J. H. Offenberg, W. Wang, M. Claeys, Formation of 2-methyl tetrols and 2-methylglyceric acid in secondary organic aerosol from laboratory irradiated isoprene/NO_X/SO_2/air mixtures and their detection in ambient $PM_{2.5}$ samples collected in the eastern United States. *Atmos. Environ.* **39**, 5281–5289 (2005).
79. J. H. Kroll, N. L. Ng, S. M. Murphy, R. C. Flagan, J. H. Seinfeld, Secondary organic aerosol formation from isoprene photooxidation under high-NO_x conditions. *Geophys. Res. Lett.* **32**, L18808 (2005).
80. T. E. Kleindienst, E. O. Edney, M. Lewandowski, J. H. Offenberg, M. Jaoui, Secondary organic carbon and aerosol yields from the irradiations of isoprene and α-pinene in the presence of NO_x and SO_2. *Environ. Sci. Technol.* **40**, 3807–3812 (2006).
81. A. W. H. Chan, M. N. Chan, J. D. Surratt, P. S. Chhabra, C. L. Loza, J. D. Crounse, L. D. Yee, R. C. Flagan, P. O. Wennberg, J. H. Seinfeld, Role of aldehyde chemistry and NO_x concentrations in secondary organic aerosol formation. *Atmos. Chem. Phys.* **10**, 7169–7188 (2010).
82. K. Sato, S. Nakao, C. H. Clark, L. Qi, D. R. Cocker III, Secondary organic aerosol formation from the photooxidation of isoprene, 1,3-butadiene, and 2,3-dimethyl-1,3-butadiene under high NO_x conditions. *Atmos. Chem. Phys.* **11**, 7301–7317 (2011).
83. L. Brégonzio-Rozier, F. Siekmann, C. Giorio, E. Pangui, S. B. Morales, B. Temime-Roussel, A. Gratien, V. Michoud, S. Ravier, M. Cazaunau, A. Tapparo, A. Monod, J.-F. Doussin, Gaseous products and secondary organic aerosol formation during long term oxidation of isoprene and methacrolein. *Atmos. Chem. Phys.* **15**, 2953–2968 (2015).
84. H. Zhang, J. D. Surratt, Y. H. Lin, J. Bapat, R. M. Kamens, Effect of relative humidity on SOA formation from isoprene/NO photooxidation: Enhancement of 2-methylglyceric acid and its corresponding oligoesters under dry conditions. *Atmos. Chem. Phys.* **11**, 6411–6424 (2011).
85. C. H. Clark, M. Kacarab, S. Nakao, A. Asa-Awuku, K. Sato, D. R. Cocker III, Temperature effects on secondary organic aerosol (SOA) from the dark ozonolysis and photo-oxidation of isoprene. *Environ. Sci. Technol.* **50**, 5564–5571 (2016).
86. R. H. Schwantes, S. M. Charan, K. H. Bates, Y. Huang, T. B. Nguyen, H. Mai, W. Kong, R. C. Flagan, J. H. Seinfeld, Low-volatility compounds contribute significantly to isoprene secondary organic aerosol (SOA) under high-NO_x conditions. *Atmos. Chem. Phys.* **19**, 7255–7278 (2019).
87. Z. Liu, M. Ge, W. Wang, Uptake of isoprene, methacrylic acid and methyl methacrylate into aqueous solutions of sulfuric acid and hydrogen peroxide. *J. Environ. Sci.* **24**, 1947–1953 (2012).
88. Z. Liu, L.-Y. Wu, T.-H. Wang, M.-F. Ge, W.-G. Wang, Uptake of methacrolein into aqueous solutions of sulfuric acid and hydrogen peroxide. *J. Phys. Chem. A* **116**, 437–442 (2012).
89. Z. Liu, M. Ge, W. Wang, S. Yin, S. Tong, The uptake of 2-methyl-3-buten-2-ol into aqueous mixed solutions of sulfuric acid and hydrogen peroxide. *Phys. Chem. Chem. Phys.* **13**, 2069–2075 (2011).
90. Q. Liu, W. Wang, Z. Liu, T. Wang, L. Wu, M. Ge, Organic hydroperoxide formation in the acid-catalyzed heterogeneous oxidation of aliphatic alcohols with hydrogen peroxide. *RSC Adv.* **4**, 19716–19724 (2014).
91. M. Claeys, W. Wang, A. Clon, I. Kourtchev, A. Gelencsér, W. Maenhaut, Formation of secondary organic aerosols from isoprene and its gas-phase oxidation products through reaction with hydrogen peroxide. *Atmos. Environ.* **38**, 4093–4098 (2004).
92. A. G. Carlton, B. J. Turpin, H.-J. Lim, K. E. Altieri, S. Seitzinger, Link between isoprene and secondary organic aerosol (SOA): Pyruvic acid oxidation yields low volatility organic acids in clouds. *Geophys. Res. Lett.* **33**, L06822 (2006).
93. H. O. T. Pye, A. Nenes, B. Alexander, A. P. Ault, M. C. Barth, S. L. Clegg, J. L. Collett Jr., K. M. Fahey, C. J. Hennigan, H. Herrmann, M. Kanakidou, J. T. Kelly, I.-T. Ku, V. F. McNeill, N. Riemer, T. Schaefer, G. Shi, A. Tilgner, J. T. Walker, T. Wang, R. Weber, J. Xing, R. A. Zaveri, A. Zuend, The acidity of atmospheric particles and clouds. *Atmos. Chem. Phys.* **20**, 4809–4888 (2020).
94. G. McFiggans, T. F. Mentel, J. Wildt, I. Pullinen, S. Kang, E. Kleist, S. Schmitt, M. Springer, R. Tillmann, C. Wu, D. Zhao, M. Hallquist, C. Faxon, M. L. Breton, Å. M. Hallquist, D. Simpson, R. Bergström, M. E. Jenkin, M. Ehn, J. A. Thornton, M. R. Alfarra, T. J. Bannan, C. J. Percival, M. Priestley, D. Topping, A. Kiendler-Scharr, Secondary organic aerosol reduced by mixture of atmospheric vapours. *Nature* **565**, 587–593 (2019).
95. E. A. Marais, D. J. Jacob, J. L. Jimenez, P. Campuzano-Jost, D. A. Day, W. Hu, J. Krechmer, L. Zhu, P. S. Kim, C. C. Miller, J. A. Fisher, K. Travis, K. Yu, T. F. Hanisco, G. M. Wolfe, H. L. Arkinson, H. O. T. Pye, K. D. Froyd, J. Liao, V. F. McNeill, Aqueous-phase mechanism for secondary organic aerosol formation from isoprene: Application to the southeast United States and co-benefit of SO_2 emission controls. *Atmos. Chem. Phys.* **16**, 1603–1618 (2016).
96. J. P. Mulcahy, C. Jones, A. Sellar, B. Johnson, I. A. Boutle, A. Jones, T. Andrews, S. T. Rumbold, J. Mollard, N. Bellouin, C. E. Johnson, K. D. Williams, D. P. Grosvenor, D. T. McCoy, Improved aerosol processes and effective radiative forcing in HadGEM3 and UKESM1. *J. Adv. Model. Earth Syst.* **10**, 2786–2805 (2018).
97. G. W. Mann, K. S. Carslaw, D. V. Spracklen, D. A. Ridley, P. T. Manktelow, M. P. Chipperfield, S. J. Pickering, C. E. Johnson, Description and evaluation of GLOMAP-mode: A modal global aerosol microphysics model for the UKCA composition-climate model. *Geosci. Model Dev.* **3**, 519–551 (2010).
98. S. J. Ghan, Technical note: Estimating aerosol effects on cloud radiative forcing. *Atmos. Chem. Phys.* **13**, 9971–9974 (2013).
99. S. J. Pai, C. L. Heald, J. R. Pierce, S. C. Farina, E. A. Marais, J. L. Jimenez, P. Campuzano-Jost, B. A. Nault, A. M. Middlebrook, H. Coe, J. E. Shilling, R. Bahreini, J. H. Dingle, K. Vu, An evaluation of global organic aerosol schemes using airborne observations. *Atmos. Chem. Phys.* **20**, 2637–2665 (2020).

100. E. Canaval, D. B. Millet, I. Zimmer, T. Nosenko, E. Georgii, E. M. Partoll, L. Fischer, H. D. Alwe, M. Kulmala, T. Karl, J.-P. Schnitzler, A. Hansel, Rapid conversion of isoprene photooxidation products in terrestrial plants. *Commun. Earth Environ.* **1**, 44 (2020).
101. A.-K. Bernhammer, M. Breitenlechner, F. N. Keutsch, A. Hansel, Technical note: Conversion of isoprene hydroxy hydroperoxides (ISOPOOHs) on metal environmental simulation chamber walls. *Atmos. Chem. Phys.* **17**, 4053–4062 (2017).

Acknowledgments
Funding: This research has received funding from the Swiss National Science Foundation (grant no. 200020_172602), the European Union's Horizon 2020 Research and Innovation programme through the EUROCHAMP-2020 Infrastructure Activity under grant agreement no. 730997, the Swiss Innovation Agency Innosuisse, the Swiss Competence Center for Energy Research SCCER BIOSWEET, and the Energy System Integration (ESI) platform at the Paul Scherrer Institute. **Author contributions:** J.D. and U.B. conceived the original idea of the project. U.B. provided funds, instruments, and supercomputing service. H.L., G.W., and J.D. designed, constructed, and prepared the WFR facility. H.L. and I.E.H. designed the research. H.L., D.S., S.B., J.K., and F.M. performed data collection. H.L. performed data analysis and interpretation. A.R. and H.G. performed the global simulation. H.L. drafted the manuscript. All coauthors commented on the results and participated in the writing and critical revision of the manuscript. **Competing interests:** The authors declare that they have no competing interests. **Data and materials availability:** All data needed to evaluate the conclusions in the paper are present in the paper and/or the Supplementary Materials. The experimental data are available at Zenodo (DOI: 10.5281/zenodo.4498915). Additional data related to this paper may be requested from the authors.

Submitted 13 August 2020
Accepted 4 February 2021
Published 24 March 2021
10.1126/sciadv.abe2952

Citation: H. Lamkaddam, J. Dommen, A. Ranjithkumar, H. Gordon, G. Wehrle, J. Krechmer, F. Majluf, D. Salionov, J. Schmale, S. Bjelić, K. S. Carslaw, I. El Haddad, U. Baltensperger, Large contribution to secondary organic aerosol from isoprene cloud chemistry. *Sci. Adv.* **7**, eabe2952 (2021).